





0144285

NACA RM L53L18a

~~CONFIDENTIAL~~

## NATIONAL ADVISORY COMMITTEE FOR AERONAUTICS

## RESEARCH MEMORANDUM

WIND-TUNNEL INVESTIGATION AT HIGH SUBSONIC  
SPEEDS TO DETERMINE THE ROLLING DERIVATIVES OF TWO  
WING-FUSELAGE COMBINATIONS HAVING TRIANGULAR WINGS,  
INCLUDING A SEMIEMPIRICAL METHOD OF ESTIMATING  
THE ROLLING DERIVATIVES

By James W. Wiggins

## SUMMARY

An investigation was conducted in the Langley high-speed 7- by 10-foot tunnel to determine the rolling stability derivatives of two wing-body configurations having triangular wings. One wing had a leading-edge sweep angle of  $45^\circ$ , an aspect ratio of 4, and an NACA 65A006 airfoil section. The second wing had a leading-edge sweep angle of  $60^\circ$ , an aspect ratio of 2.31, and an NACA 65A003 airfoil section. The results from the  $45^\circ$  (6-percent-thick) wing indicate an appreciable loss of damping in roll  $C_{l_p}$  at the higher test angles of attack, and particularly at the higher Mach numbers. However, no negative damping (positive values of damping in roll  $C_{l_p}$ ) was encountered within the ranges of variables covered in the tests. Negative damping at values of wing-tip helix angle  $\frac{pb}{2V}$  near zero was encountered with the  $60^\circ$  (3-percent-thick) wing at a Mach number of 0.85 and at angles of attack above  $10.5^\circ$ ; however, this negative damping was eliminated by notches in the wing leading edge at the 60-percent-semispan station.

Semiempirical methods are developed herein for estimating the derivatives  $C_{l_p}$  (rolling moment due to rolling),  $C_{n_p}$  (yawing moment due to rolling), and  $C_{y_p}$  (lateral force due to rolling) through the test angle-of-attack range. Predictions based on these methods are in good agreement with experiment for the two triangular wings over the angle-of-attack range and Mach number range investigated.

~~CONFIDENTIAL~~

440054-717

## INTRODUCTION

The present investigation is a continuation of a program being conducted in the Langley high-speed 7- by 10-foot tunnel to determine the effects of wing geometry on the rolling stability characteristics of wing-body combinations at Mach numbers up to 0.95. Reported herein are results for two wing-fuselage combinations having triangular wings along with a semiempirical method for estimating  $C_{np}$  and  $C_{yp}$  through the test angle-of-attack range. One wing had a leading-edge sweep angle of  $60^\circ$ , an aspect ratio of 2.31, and an NACA 65A003 airfoil section. The other wing had a leading-edge sweep angle of  $45^\circ$ , an aspect ratio of 4, and an NACA 65A006 airfoil section. Tests at selected angles of attack were repeated for the  $60^\circ$  triangular wing with notches in the leading edges of the wing at the 60-percent-semispan station. The location of the notch was determined from unpublished low-speed data on a  $45^\circ$  swept wing.

The longitudinal and lateral stability characteristics of the  $60^\circ$  and  $45^\circ$  triangular wings are presented in references 1 and 2, respectively, and the damping in roll  $C_{lp}$  for the  $60^\circ$  wing at a Mach number of 0.85 is presented in reference 3. Body-alone characteristics in pitch and sideslip are presented in references 4 and 5, respectively.

## SYMBOLS

The stability system of axes used for the presentation of the results, together with an indication of the positive forces, moments, velocities, and angles, is presented in figure 1. All moments are referred to the projection of the quarter-chord point of the wing mean aerodynamic chord on the fuselage center line.

$C_l$       rolling-moment coefficient,  $\frac{\text{Rolling moment}}{qSb}$

$C_n$       yawing-moment coefficient,  $\frac{\text{Yawing moment}}{qSb}$

$C_y$       lateral-force coefficient,  $\frac{\text{Lateral force}}{qS}$

$C_D$       drag coefficient,  $\frac{\text{Drag}}{qS}$

$C_L$  lift coefficient,  $\frac{\text{Lift}}{qS}$

$q$  dynamic pressure,  $\frac{\rho V^2}{2}$ , lb/sq ft

$\rho$  mass density of air, slugs/cu ft

$V$  free-stream velocity, ft/sec

$M$  Mach number

$R$  Reynolds number

$S$  wing area, sq ft

$b$  wing span, ft

$\bar{c}$  mean aerodynamic chord, ft

$\alpha$  angle of attack, deg

$\frac{pb}{2V}$  wing-tip helix angle, radians

$$C_{L_p} = \frac{\partial C_L}{\partial \frac{pb}{2V}} \text{ per radian}$$

$$C_{n_p} = \frac{\partial C_n}{\partial \frac{pb}{2V}} \text{ per radian}$$

$$C_{Y_p} = \frac{\partial C_Y}{\partial \frac{pb}{2V}} \text{ per radian}$$

#### MODEL AND APPARATUS

A drawing of the models investigated is shown in figure 2. The two wings were constructed of 24S-T aluminum alloy: One wing had a leading-edge sweep of  $60^\circ$ , aspect ratio of 2.31, and an NACA 65A003 airfoil section and the other wing had a leading-edge sweep of  $45^\circ$ , aspect ratio of 4, and an NACA 65A006 airfoil section. Location of the leading-edge

~~CONFIDENTIAL~~

notch on the  $60^\circ$  wing was determined from unpublished low-speed data on a  $45^\circ$  swept wing. The wings were attached to the body in a midwing position. The geometric characteristics of the body are presented in reference 4.

The models were tested on the forced-roll sting support shown in figure 3. Details of the operation of the roll sting and the technique of recording the data are discussed in reference 6. Various angles of attack were obtained by use of offset sting adapters in the sting behind the model (fig. 3).

The forces and moments were measured on an internally mounted electrical strain-gage balance.

#### TESTS AND CORRECTIONS

The forced-roll tests were made in the Langley high-speed 7- by 10-foot tunnel through a Mach number range from 0.50 to 0.95, and through an angle-of-attack range from  $0^\circ$  to about  $13^\circ$ . Tests on the  $60^\circ$  triangular wing were repeated at angles of attack of approximately  $10.5^\circ$  and  $12.5^\circ$  and at Mach numbers of 0.70, 0.80, 0.85, and 0.91 with notches in the leading edge of the wing at the 60-percent-semispan station. The variation of maximum test  $\frac{pb}{2V}$  with Mach number is presented in figure 4

and the variation with Mach number of the mean test Reynolds number (based on the mean aerodynamic chord of the wing) is presented in figure 5 for the two wing-fuselage configurations.

The blocking corrections applied to the dynamic pressure and Mach number were determined by the velocity-ratio method of reference 7. An investigation of the jet-boundary corrections to the rolling derivatives by the method of reference 8 indicated that these corrections were negligible. Angle of attack and drag were corrected for jet boundary effects by the method of reference 9. Tare tests were made at zero angle of attack with and without a simulated offset coupling behind the model and the effects were found to be negligible.

The data presented have been corrected for inertia forces and moments that were introduced as the model was rotated, consideration also being given to deflections of the entire support system under aerodynamic loads. The effects of wing distortion are believed to be small and, therefore, the data presented have not been corrected to account for aeroelastic distortion. The angle of attack at the plane of symmetry has been corrected for the deflection of the model and support system under load.

## RESULTS AND DISCUSSION

The results of the investigation are presented in the figures as follows:

Results	Figure
$C_l$ , $C_n$ , and $C_y$ against $\frac{pb}{2V}$ . . . . .	6
$C_{l_p}$ , $C_{n_p}$ , and $C_{y_p}$ against $\alpha$ . . . . .	7
$C_{l_p}$ against $\alpha$ at $\frac{pb}{2V} \approx 0$ and $\pm 0.06$ . . . . .	8
Drag due to lift against $\alpha$ . . . . .	9
$C_{l_p}$ against $M$ . . . . .	10
$C_{l_p}$ against $\alpha$ compared with calculations . . . . .	11 and 12
$C_{n_p}$ against $\alpha$ compared with calculations . . . . .	13 and 14
$C_{y_p}$ against $\alpha$ compared with calculations . . . . .	15

Figure 6 presents plots of  $C_l$ ,  $C_n$ , and  $C_y$  against  $\frac{pb}{2V}$  at two angles of attack ( $\alpha = 10.5^\circ$  and  $12.5^\circ$ ) for the  $60^\circ$  (3-percent-thick) wing. The nonlinearities indicated for the clean-wing configuration occurred only at these angles of attack and the data at lower angles of attack were linear over the  $\frac{pb}{2V}$  range investigated. The data for the  $45^\circ$  (6-percent-thick) wing were linear at all test angles of attack.

## Experimental Rolling Derivatives

Rolling moment due to rolling.— The variation with angle of attack of the damping-in-roll derivative  $C_{l_p}$ , measured near zero values of  $\frac{pb}{2V}$ , is presented in figure 7(a) for the two configurations. The damping in roll  $C_{l_p}$  at the lower Mach numbers shows reasonably good agreement with the low-speed wing-fuselage data of references 10 and 11. The present results indicate a loss in damping for the  $45^\circ$  (6-percent-thick) wing as the angle of attack is increased; however, the damping in roll for the  $60^\circ$  (3-percent-thick) wing increases slightly with an increase in angle of attack up to about  $8^\circ$ . Above  $8^\circ$  the damping decreases somewhat, and at a Mach number of 0.85 a severe decrease is apparent with the configuration showing negative damping (positive values of  $C_{l_p}$ ).

above an angle of attack of about  $10.5^\circ$ . This adverse rolling effect - occurs only at values of  $\frac{pb}{2V}$  near zero with a stable condition indicated at higher rolling velocities (figs. 6(a) and 8). At an angle of attack of  $10.5^\circ$  (fig. 6(a)), a small hysteresis loop is apparent near zero  $\frac{pb}{2V}$  for the  $60^\circ$  clean-wing configuration at a Mach number of 0.85. (The data were obtained by rolling from the extreme negative values of  $\frac{pb}{2V}$  to the extreme positive values of  $\frac{pb}{2V}$ , then back through the  $\frac{pb}{2V}$  range.) These nonlinearities and the hysteresis near zero  $\frac{pb}{2V}$  at these angles of attack may not greatly affect the controllability of a similar airplane configuration; however, these conditions may result in dynamic instability and wing-dropping problems in this region. These nonlinearities and the hysteresis are also indicated for an unswept wing having a taper ratio of 0.6 (ref. 3).

In an attempt to eliminate these unstable conditions indicated by  $C_{lp}$ , the  $60^\circ$  wing was tested at angles of attack of  $10.5^\circ$  and  $12.5^\circ$  with a notch in the leading edge of the wing at the 60-percent-semispan station, since the data of reference 2 show that the notch eliminated a pitch-up that occurred at about the same angle of attack. The results herein (figs. 6(a) and 7(a)) show that the notched configuration remained stable throughout the test  $\frac{pb}{2V}$  range at these angles of attack.

Yawing moment due to rolling.- The results presented in figure 7(b) show negative values of yawing moment due to rolling  $C_{np}$  at angles of attack above about  $10.5^\circ$  for the  $60^\circ$  clean-wing configuration at a Mach number of 0.85. These negative slopes occur only near zero values of  $\frac{pb}{2V}$  and the slope is about neutral or slightly positive at the higher rolling velocities (fig. 6(b)). Positive values of  $C_{np}$  resulted when the notch was added to the wing. Other than at angles of attack above  $10.5^\circ$  at a Mach number of 0.85, both wing-fuselage combinations showed zero or positive values of  $C_{np}$  through the test angle-of-attack range and Mach number range (fig. 7(b)). Low-speed results of reference 10 agree with the present results of the  $60^\circ$  triangular wing at the lower Mach numbers.

Lateral force due to rolling.- The variation of  $C_{Yp}$  with angle of attack for the two wings are shown in figure 7(c). Positive values

of  $C_{Y_p}$  are indicated through the test angle-of-attack range for the  $60^\circ$  wing and the effects of the notch are seen to be small. The results for the  $45^\circ$  (6-percent-thick) wing show positive values of  $C_{Y_p}$  at the lower angles of attack and zero or slightly negative values at the higher test angles of attack.

### Estimation of Rolling Derivatives

Rolling moment due to rolling.- The experimental variation of  $C_{l_p}$  at zero angle of attack with Mach number is compared with an estimated variation in figure 10. The calculated variation was determined by the methods of references 12 and 13. The agreement shown is reasonably good except for the  $45^\circ$  (6-percent-thick) wing at the higher subsonic Mach numbers where experimental  $C_{l_p}$  decreases with increasing Mach number - similar to the lift-curve-slope results presented in reference 1.

A comparison of the variation of  $C_{l_p}$  with angle of attack as determined by experiment and as calculated from available procedures (for example, method 3 of ref. 11), using the experimental lift-curve slopes of references 1 and 2, is shown in figure 11 for the two configurations. Estimated values of  $C_{l_p}$  at zero angle of attack (refs. 12 and 13 and presented in fig. 10 of this paper) were used in the determination of the effects of angle of attack. The quantitative agreement is only fair although the experimental and predicted results show about the same trends.

Inasmuch as the nonlinearity of  $C_{l_p}$  with angle of attack is undoubtedly a function of changes in spanwise location of the center of load, it would appear that root bending moments would be more appropriate than lift data in predicting the variation of  $C_{l_p}$  with angle of attack. Bending-moment data are not available for either of the wings considered herein; however, such data have been obtained (unpublished) for a  $45^\circ$  delta wing having an NACA 65A003 airfoil section. These data were obtained in the Langley high-speed 7- by 10-foot tunnel by the transonic-bump technique up to a Mach number of 1.18 at angles of attack up to  $30^\circ$ . In figure 12 the variation of  $C_{l_p}$  with angle of attack, determined by using bending-moment data instead of lift-curve slopes, is presented at several Mach numbers. For a Mach number of 1.18,  $C_{l_p}$  at zero angle of attack was determined from reference 14. Also shown in figure 12 are experimental values of  $C_{l_p}$  for the  $45^\circ$  (6-percent-thick) wing at Mach numbers of 0.70 and 0.90. The agreement is shown to be better when the

predictions are based on bending-moment data rather than lift data (compare figs. 11 and 12). Inasmuch as the wings had different airfoil sections, the agreement may be somewhat fortuitous; however, the predictions are presented herein primarily to give an indication of the behavior of  $C_{lp}$  at high angles of attack and at transonic and supersonic speeds.

Yawing moment due to rolling.— The present available method for estimating  $C_{np}$  through the test angle-of-attack range considers only untapered wings (ref. 15). However, as is shown in reference 15,  $C_{np}$  depends upon the rate of change of drag coefficient with angle of attack. If the actual rate of change of drag coefficient with angle of attack corresponds to that predicted by potential-flow theory

$$C_D = (C_D)_{C_L=0} + \frac{C_L^2}{\pi A}$$

$C_{np}$ , of course, can be predicted by the potential-flow theories of references 16 and 17. However, if, as a result of nonpotential-flow effects (for example, leading-edge separation), the rate of change of drag coefficient with angle of attack corresponds to the case of the resultant force due to angle of attack being normal to the wing chord line at all angles of attack ( $C_D = C_L \tan \alpha$ ),  $C_{np}$  will be equal to  $(-C_{lp} \tan \alpha)$ .

Intermediate flow conditions will be indicated by the actual drag variation with angle of attack in relation to the above conditions. It, therefore, should be possible to determine  $C_{np}$  for any intermediate flow

conditions if corresponding drag data are available. It should be pointed out that a rate of change of drag coefficient with angle of attack equal to or greater than that given by  $C_D = C_L \tan \alpha$  can be obtained without the resultant force being normal to the wing chord during a transition between the two types of flow. However, it is the rate of change of drag with angle of attack that determines  $C_{np}$ . The potential-flow condition would seem to be described most accurately for the wings of this report

by the triangular-wing theory of reference 16, which gives  $C_{np} = -\frac{2C_L}{3A^2}$ .

An expression applicable to an intermediate flow condition can be expressed as follows:

$$C_{np} = (-C_{lp} \tan \alpha) - K \left[ (-C_{lp} \tan \alpha) - \left( -\frac{2C_L}{3A^2} \right) \right] \quad (1)$$

where  $K$  is the constant of proportionality and can be determined from the drag data as follows:

$$K = \frac{\frac{\partial}{\partial \alpha}(C_L \tan \alpha) - \frac{\partial}{\partial \alpha} \left[ C_D - (C_D)_{C_L=0} \right]_{\text{exp}}}{\frac{\partial}{\partial \alpha}(C_L \tan \alpha) - \frac{\partial}{\partial \alpha} \left( \frac{C_L^2}{\pi A} \right)} \quad (2)$$

The local slopes of drag against angle of attack were measured from figure 9.

Several methods of calculating the effects of angle of attack on  $C_{np}$  are compared with experiment at a Mach number of 0.85 for the two configurations in figure 13. The variation given by equation (1) shows the best agreement. Because of the relatively small amount of leading-edge suction developed by the wings of the present investigation (indicated in fig. 9), the values of  $C_{np}$  given by  $(-C_{lp} \tan \alpha)$  also are in good agreement with experiment. The values of  $C_{np}$  determined by using reference 15 (the increment of  $C_{np}$  due to tip suction was neglected in the consideration herein since the wings are fully tapered) are not expected to agree with the results of the present investigation since the method of reference 15 was derived for untapered wings; however, the comparison is shown herein (fig. 13) inasmuch as it does consider the influence of the drag characteristics on  $C_{np}$  for swept wings. Calculations by use of equation (1) are compared with experiment in figure 14. Experimental values of  $C_L$  and  $C_D$  and both experimental and calculated values of  $C_{lp}$  were used in the calculations. The agreement, when either experimental values or calculated values of  $C_{lp}$  are used, is reasonably good, and the negative values of  $C_{np}$  shown for the 60° triangular wing at a Mach number of 0.85 and above a test angle of attack of about 10.5° were accurately predicted when experimental  $C_{lp}$  was used in equation (1).

Lateral force due to rolling.— The variation of  $C_{yp}$  with angle of attack is presented in figure 15. The calculated variation, which shows good agreement with experiment, was determined by applying the factor  $K$

to the linear theory of reference 16. The expression for determining  $C_{Y_p}$  from reference 16, which assumes full leading-edge suction is

$$C_{Y_p} = \frac{4C_L}{3A}$$

and, for the case of zero leading-edge suction,  $C_{Y_p}$  would be equal to zero. Therefore, applying the factor  $K$  to account for leading-edge suction, the expression for determining  $C_{Y_p}$  can be written as follows:

$$C_{Y_p} = K \left( \frac{4C_L}{3A} \right) \quad (3)$$

where the values of  $C_L$  and  $C_D$  used are experimental.

#### CONCLUSIONS

An investigation conducted to determine the rolling derivatives of triangular wings, one having a leading-edge sweep angle of  $45^\circ$ , aspect ratio 4, and an NACA 65A006 airfoil section, and the other having a leading-edge sweep angle of  $60^\circ$ , aspect ratio of 2.31, and an NACA 65A003 airfoil section, indicate the following conclusions:

1. The results for the  $45^\circ$  (6-percent-thick) wing indicate an appreciable loss in damping in roll  $C_{l_p}$  at the higher angles of attack and particularly at the higher test Mach numbers; however, no negative damping (positive values of damping in roll  $C_{l_p}$ ) were encountered within the range of variables covered in the tests. Negative damping was encountered at values of wing-tip helix angle  $\frac{pb}{2V}$  near zero for the  $60^\circ$  (3-percent-thick) wing at a Mach number of 0.85 and at angles of attack above  $10.5^\circ$ .

2. For both wings, the yawing-moment-due-to-rolling derivative  $C_{n_p}$  was positive over most of the angle-of-attack range at all Mach numbers.

3. Notches in the leading edge of the  $60^\circ$  wing at the 60-percent-semispan station eliminated the negative damping (positive values of damping in roll  $C_{l_p}$ ) near zero values of  $\frac{pb}{2V}$  that was indicated at a Mach number of 0.85 and at angles of attack above  $10.5^\circ$ .

4. Semiempirical methods developed herein for estimating the rolling derivatives  $C_{l_p}$ ,  $C_{n_p}$ , and  $C_{Y_p}$  provide good agreement with experiment for the two triangular wings over the angle-of-attack range and Mach number range investigated.

Langley Aeronautical Laboratory,  
National Advisory Committee for Aeronautics,  
Langley Field, Va., December 1, 1953.

## REFERENCES

1. Fournier, Paul G.: Wind-Tunnel Investigation of the Aerodynamic Characteristics in Pitch and Sideslip at High Subsonic Speeds of a Wing-Fuselage Combination Having a Triangular Wing of Aspect Ratio 4. NACA RM L53G14a, 1953.
2. Wiggins, James W.: Wind-Tunnel Investigation at High Subsonic Speeds of the Static Longitudinal and Static Lateral Stability Characteristics of a Wing-Fuselage Combination Having a Triangular Wing of Aspect Ratio 2.31 and an NACA 65A003 Airfoil. NACA RM L53G09a, 1953.
3. Kuhn, Richard E.: Notes on Damping in Roll and Load Distribution in Roll at High Angles of Attack and High Subsonic Speed. NACA RM L53G13a, 1953.
4. Kuhn, Richard E., and Wiggins, James W.: Wind-Tunnel Investigation of the Aerodynamic Characteristics in Pitch of Wing-Fuselage Combinations at High Subsonic Speeds - Aspect-Ratio Series. NACA RM L52A29, 1952.
5. Kuhn, Richard E., and Fournier, Paul G.: Wind-Tunnel Investigation of the Static Lateral Stability Characteristics of Wing-Fuselage Combinations at High Subsonic Speeds - Sweep Series. NACA RM L52G11a, 1952.
6. Kuhn, Richard E., and Wiggins, James W.: Wind-Tunnel Investigation to Determine the Aerodynamic Characteristics in Steady Roll of a Model at High Subsonic Speeds. NACA RM L52K24, 1953.
7. Hensel, Rudolph W.: Rectangular-Wind Tunnel Blocking Corrections Using the Velocity-Ratio Method. NACA TN 2372, 1951.
8. Evans, J. M., and Fink, P. T.: Stability Derivatives. Determination of  $l_p$  by Free Oscillation. Rep. ACA-34, Australian Council for Aeronautics, Apr. 1947.
9. Gillis, Clarence L., Polhamus, Edward C., and Gray, Joseph L., Jr.: Charts for Determining Jet-Boundary Corrections for Complete Models in 7- by 10-Foot Closed Rectangular Wind Tunnels. NACA WRL-123, 1945. (Formerly NACA ARR L5G31).
10. Jaquet, Byron M., and Brewer, Jack D.: Effects of Various Outboard and Central Fins on Low-Speed Static Stability and Rolling Characteristics of a Triangular-Wing Model. NACA RM L9E18, 1949.

11. Goodman, Alex, and Adair, Glenn H.: Estimation of the Damping in Roll of Wings Through the Normal Flight Range of Lift Coefficient. NACA TN 1924, 1949.
12. Bird, John D.: Some Theoretical Low-Speed Span Loading Characteristics of Swept Wings in Roll and Sideslip. NACA Rep. 969, 1950. (Supersedes NACA TN 1839.)
13. Fisher, Lewis R.: Approximate Corrections for the Effects of Compressibility on the Subsonic Stability Derivatives of Swept Wings. NACA TN 1854, 1949.
14. Jones, Arthur L., and Alksne, Alberta: The Damping Due to Roll of Triangular, Trapezoidal, and Related Plan Forms in Supersonic Flow. NACA TN 1548, 1948.
15. Goodman, Alex, and Fisher, Lewis R.: Investigation at Low Speeds of the Effect of Aspect Ratio and Sweep on Rolling Stability Derivatives of Untapered Wings. NACA Rep. 969, 1950. (Supersedes NACA TN 1835.)
16. Ribner, Herbert S.: The Stability Derivatives of Low-Aspect-Ratio Triangular Wings at Subsonic and Supersonic Speeds. NACA TN 1423, 1947.
17. Toll, Thomas A., and Queijo, M. J.: Approximate Relations and Charts for Low-Speed Stability Derivatives of Swept Wings. NACA TN 1581, 1948.

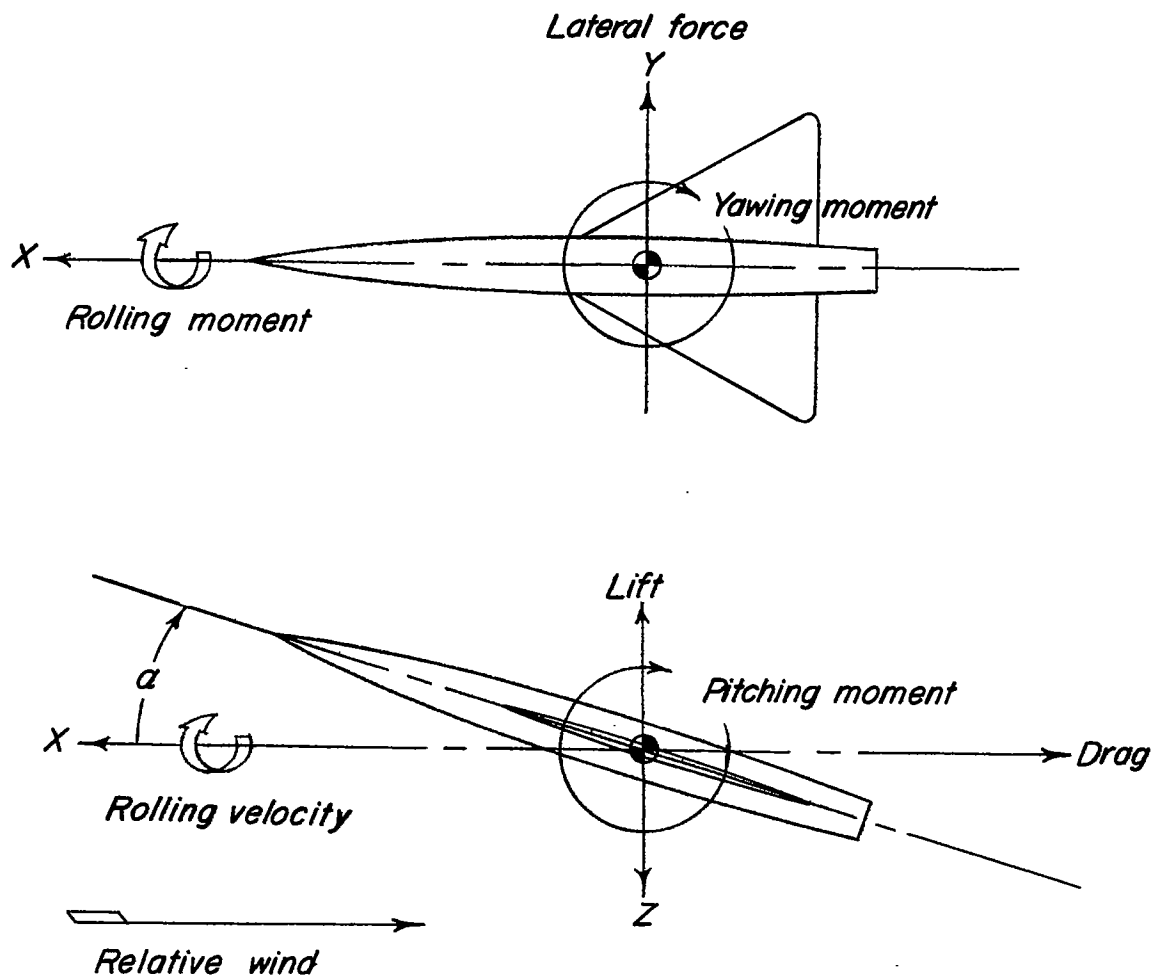


Figure 1.- System of axes used showing positive directions of forces, moments, angles, and velocities.

Wing Geometry

Area 2.25 sq ft  
Aspect ratio 2.31  
Sweep at  $\frac{3}{4}$  52.4°  
Airfoil section parallel to fuselage centerline NACA 65A003

Wing Geometry

Area 2.25 sq ft  
Aspect ratio 4.0  
Sweep at  $\frac{3}{4}$  36.9°  
Airfoil section parallel to fuselage centerline NACA 65A006

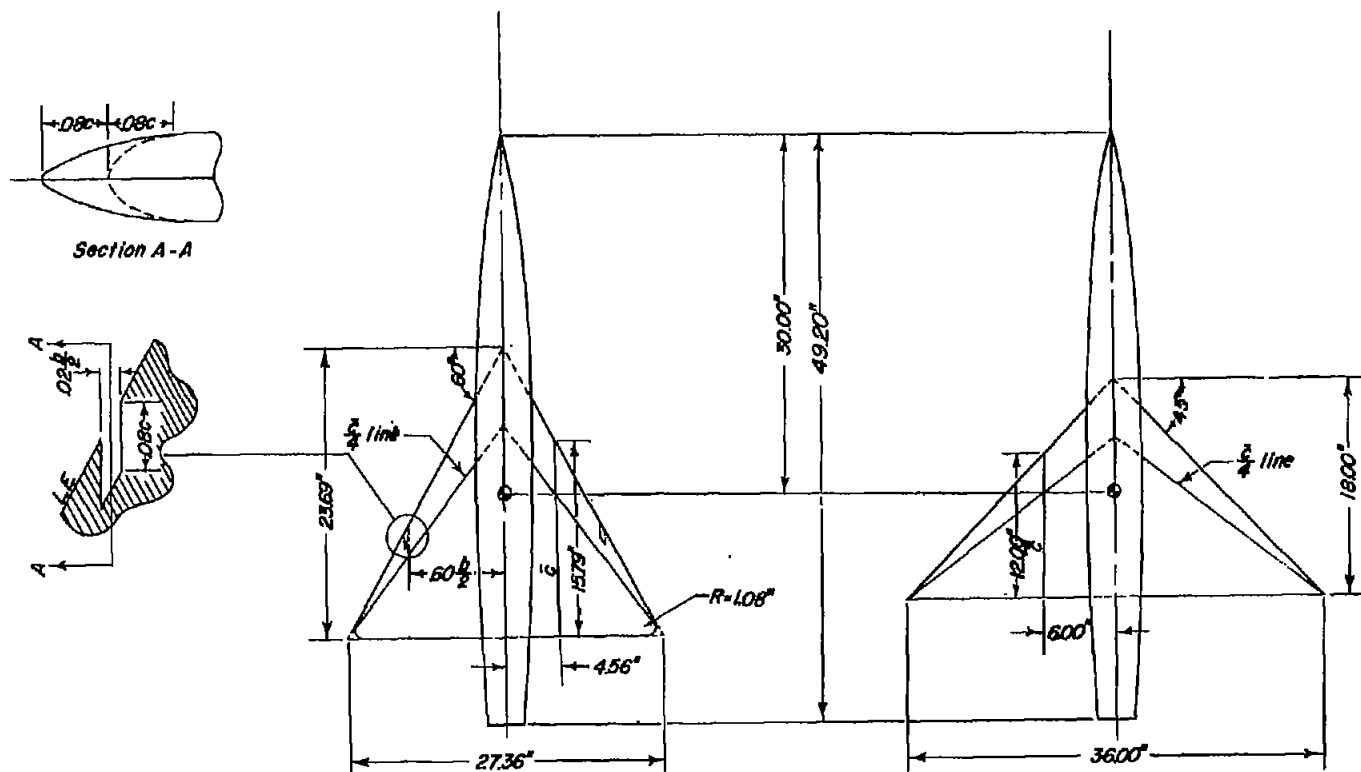


Figure 2.- Plan form of models and details of notch in the leading edge of the 60° wing.

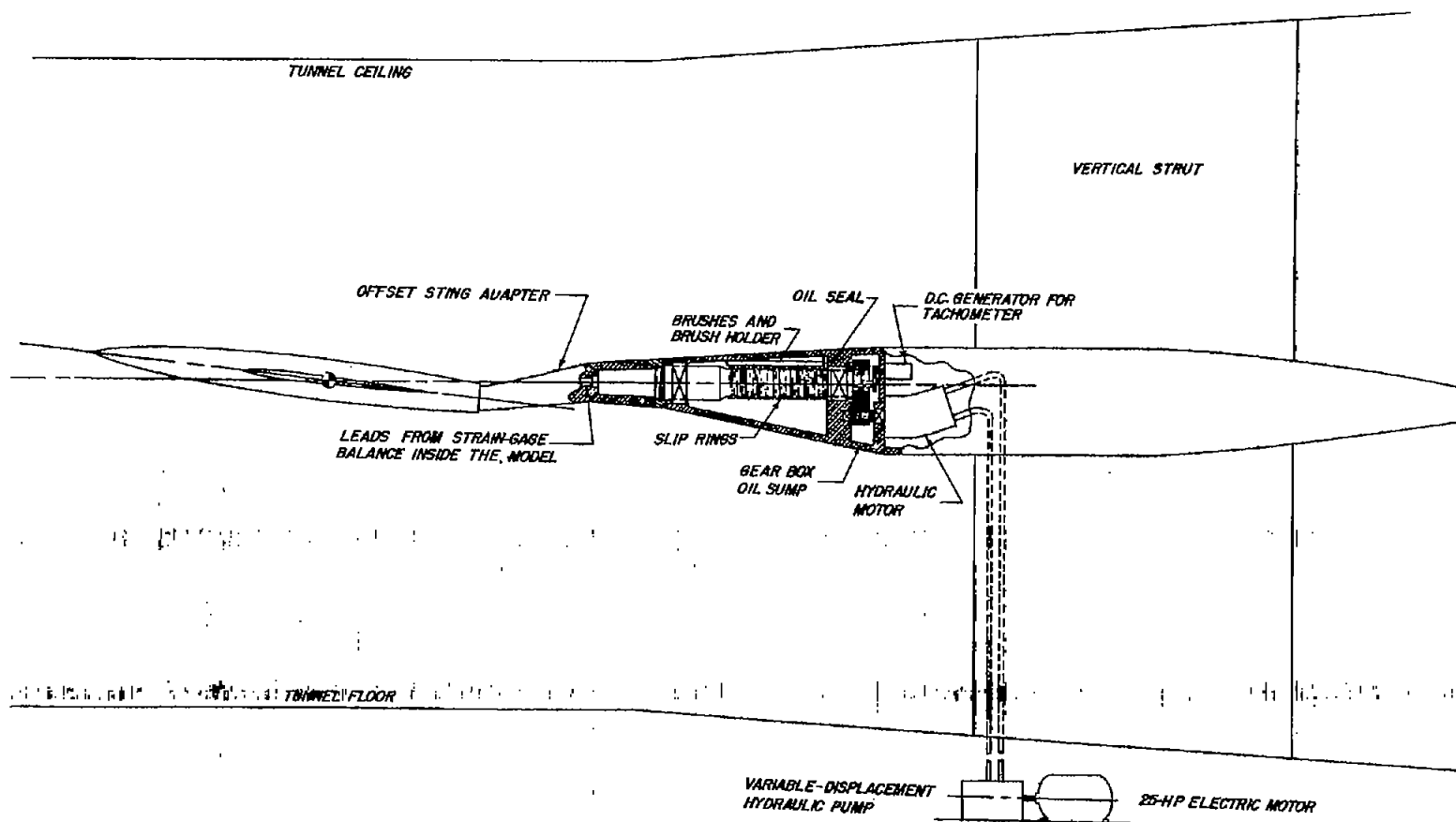


Figure 3.- General arrangement of forced-roll support system.

CONFIDENTIAL

CONFIDENTIAL

NACA RM L53L18a

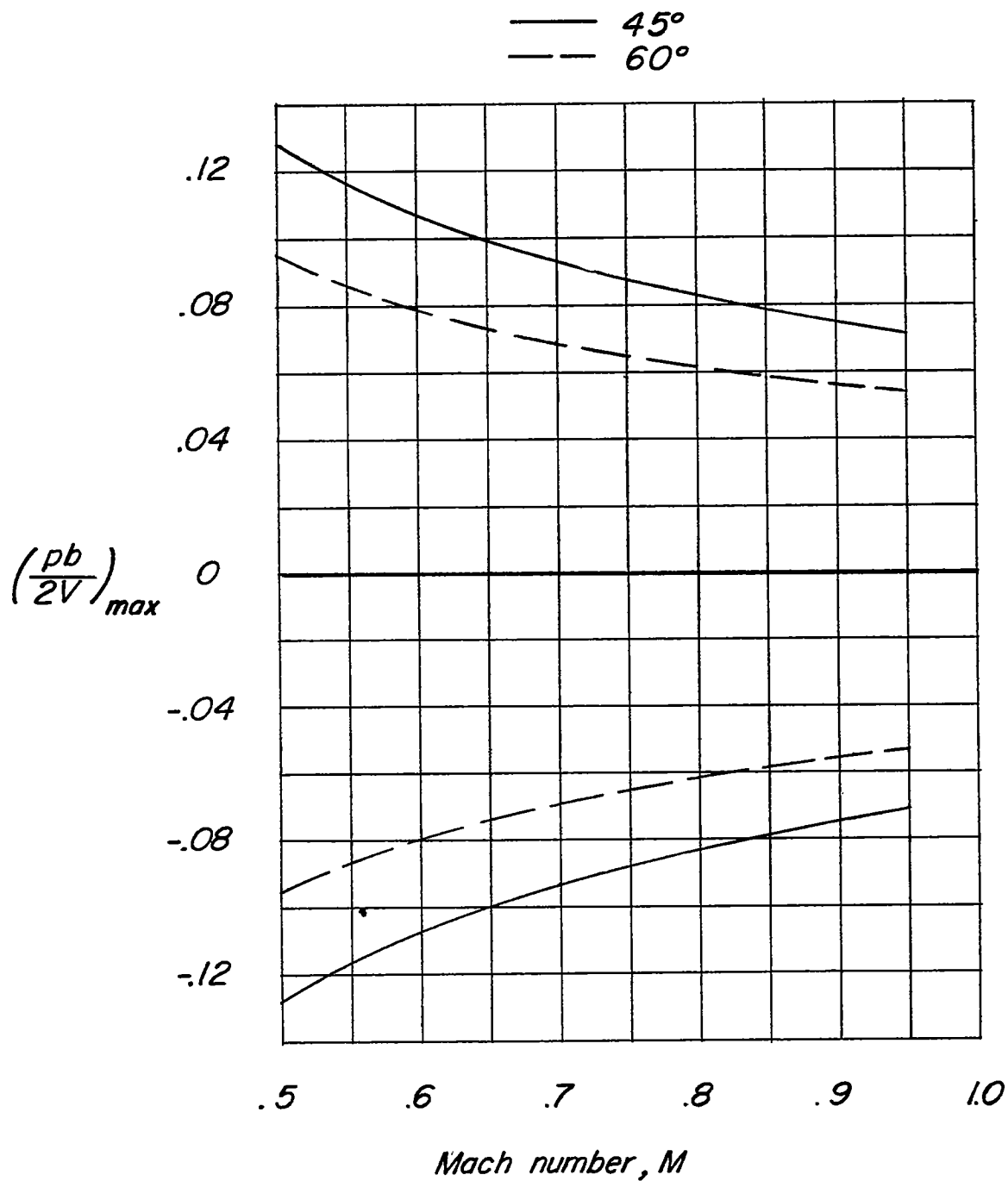


Figure 4.- Variation of maximum test  $pb/2V$  with Mach number for the two triangular wings.

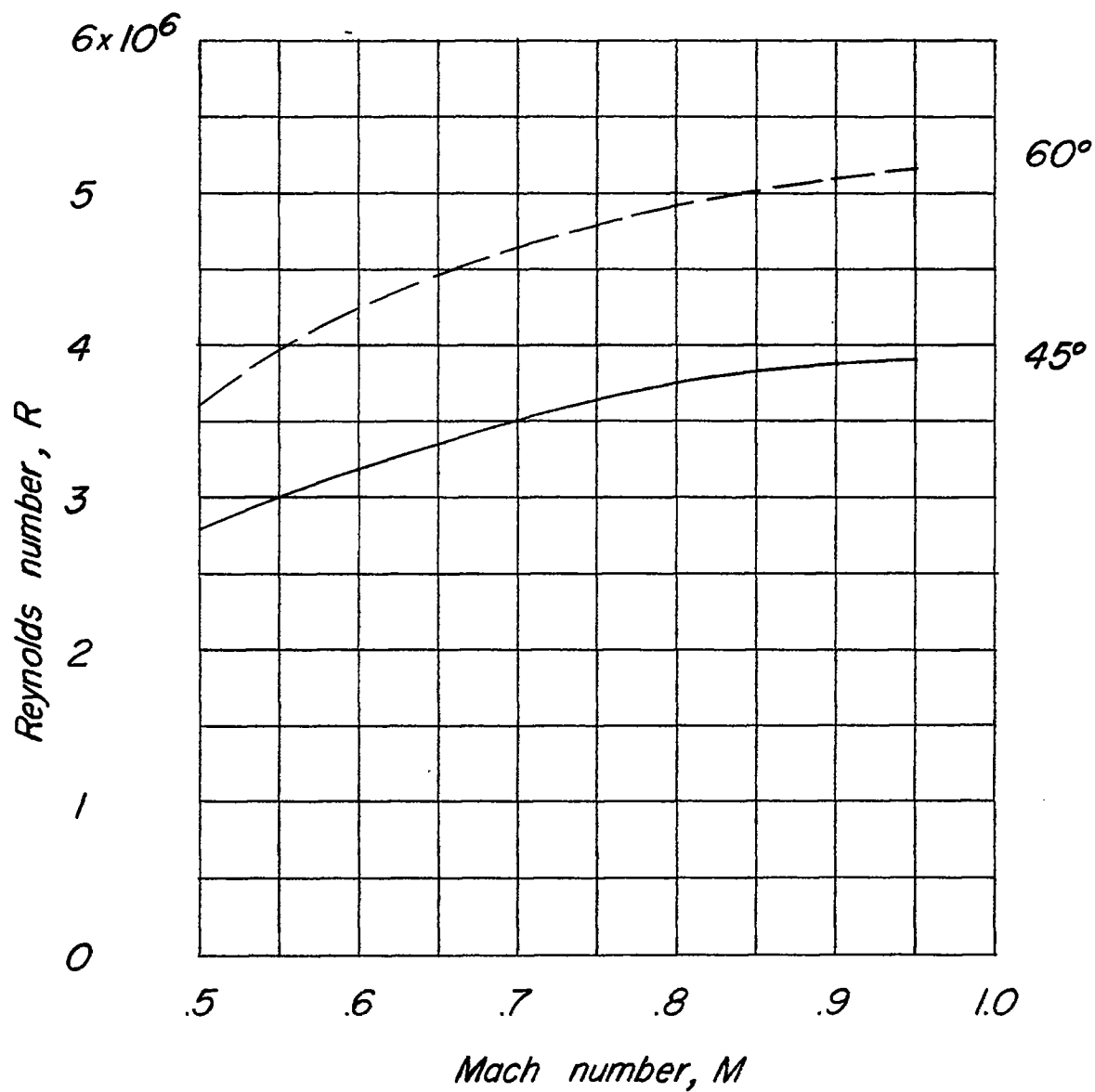
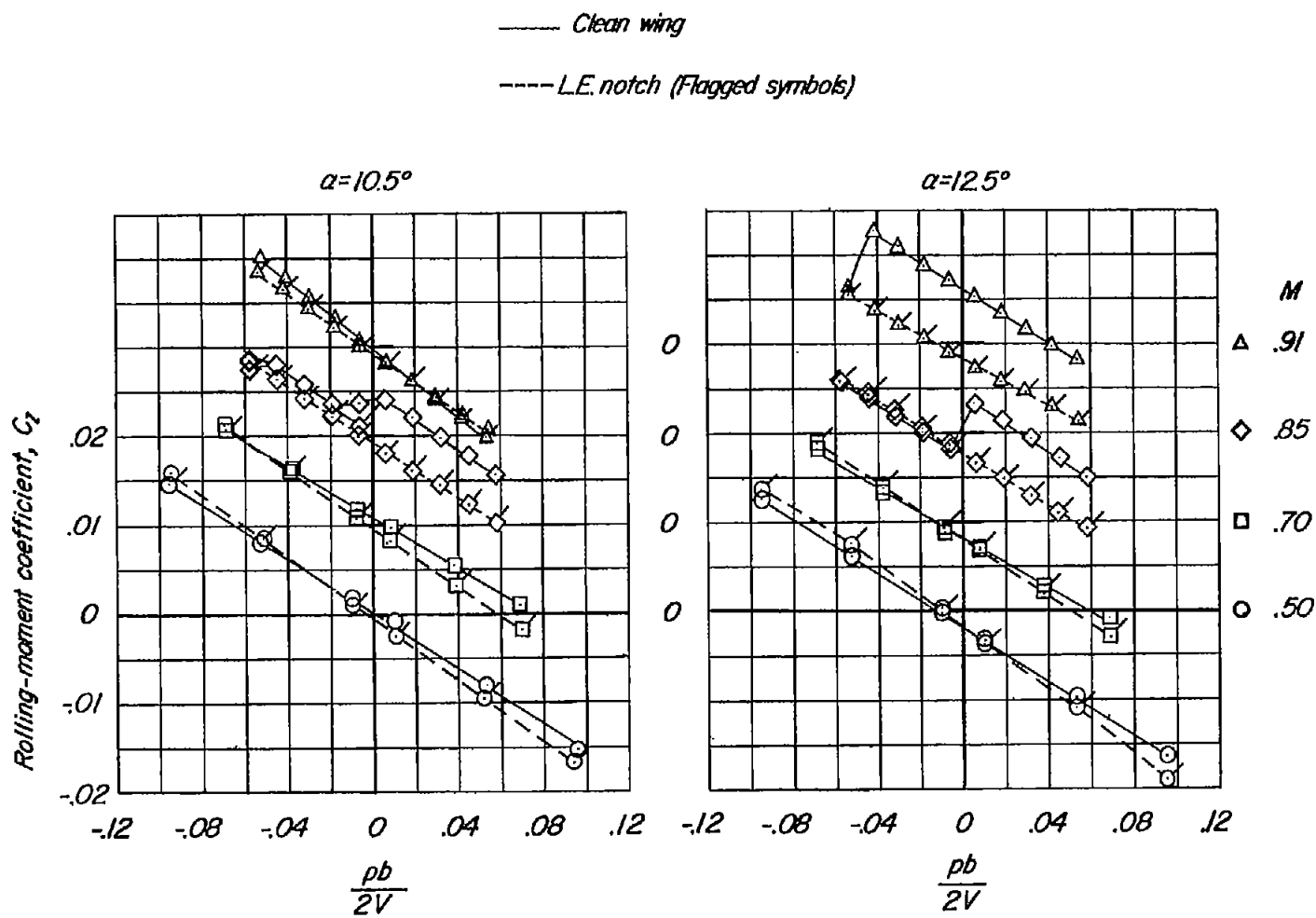


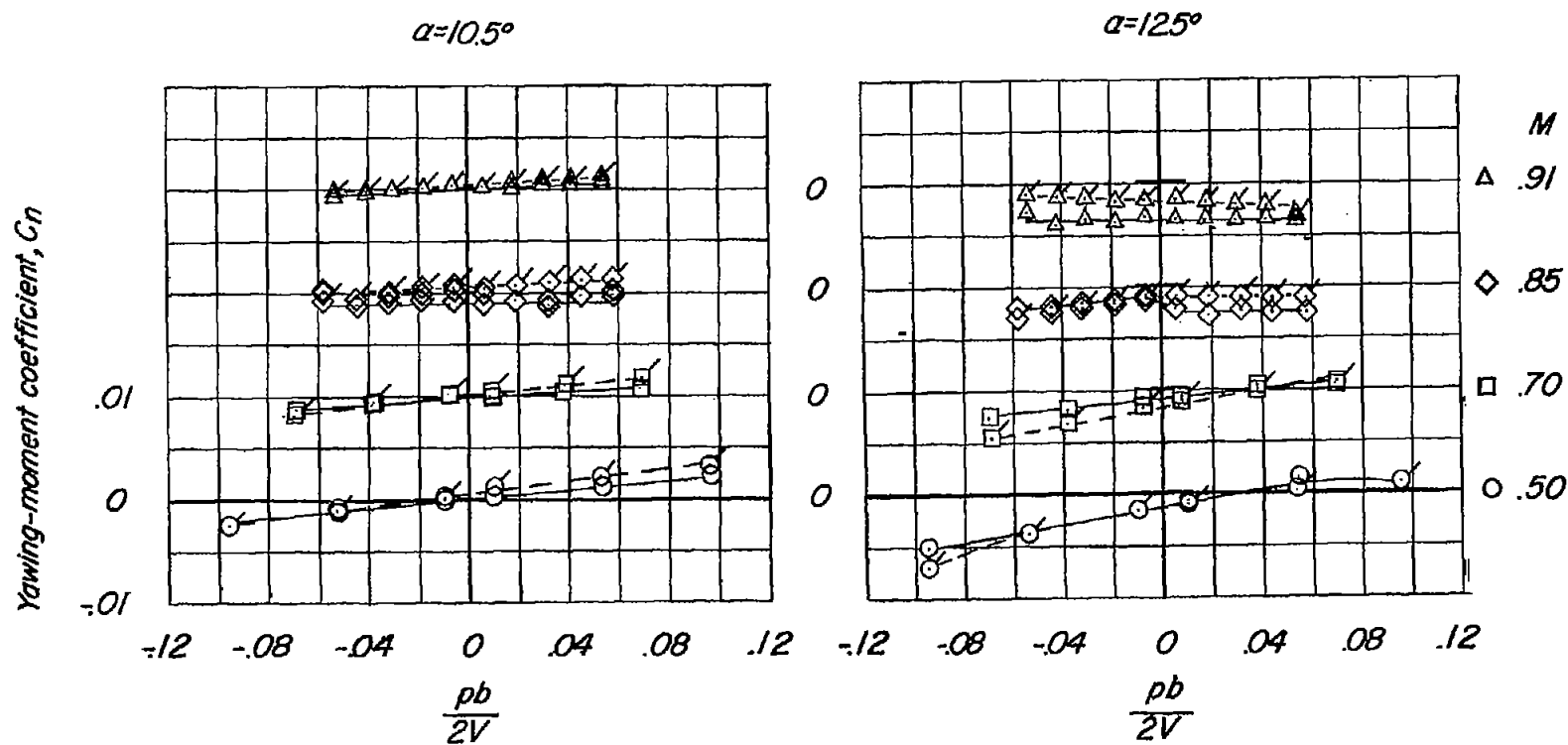
Figure 5.- Variation of mean test Reynolds number with Mach number for the two triangular wings.



(a)  $C_l$ .

Figure 6.- Variation of  $C_l$ ,  $C_n$ , and  $C_y$  with  $pb/2V$  for the  $60^\circ$  (3-percent-thick) triangular wing.

— Clean wing  
 --- LE notch (Flagged symbols)

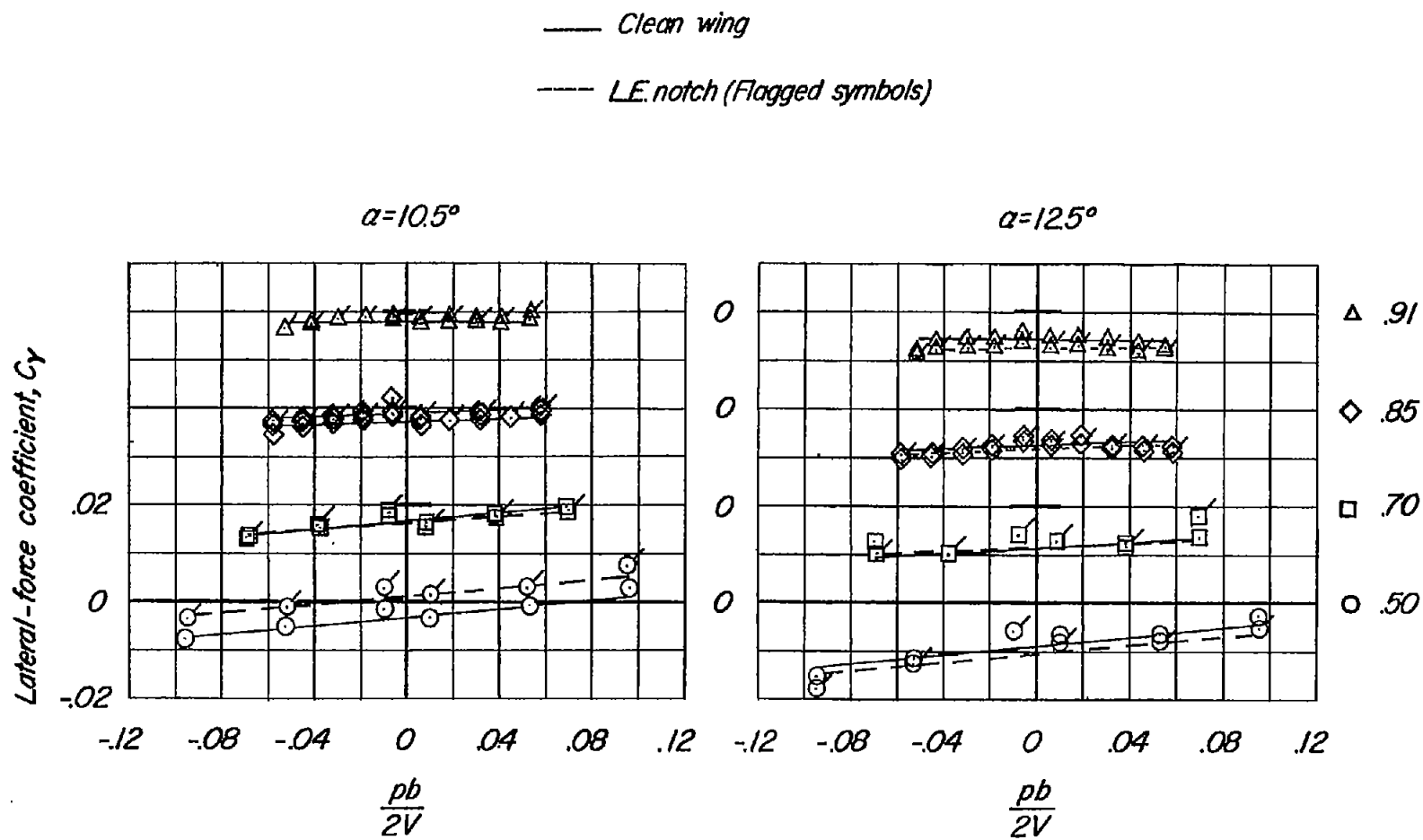


(b)  $C_n$ .

Figure 6.- Continued.

CONFIDENTIAL

NACA RM L53118a



(c)  $C_Y$ .

Figure 6.- Concluded.

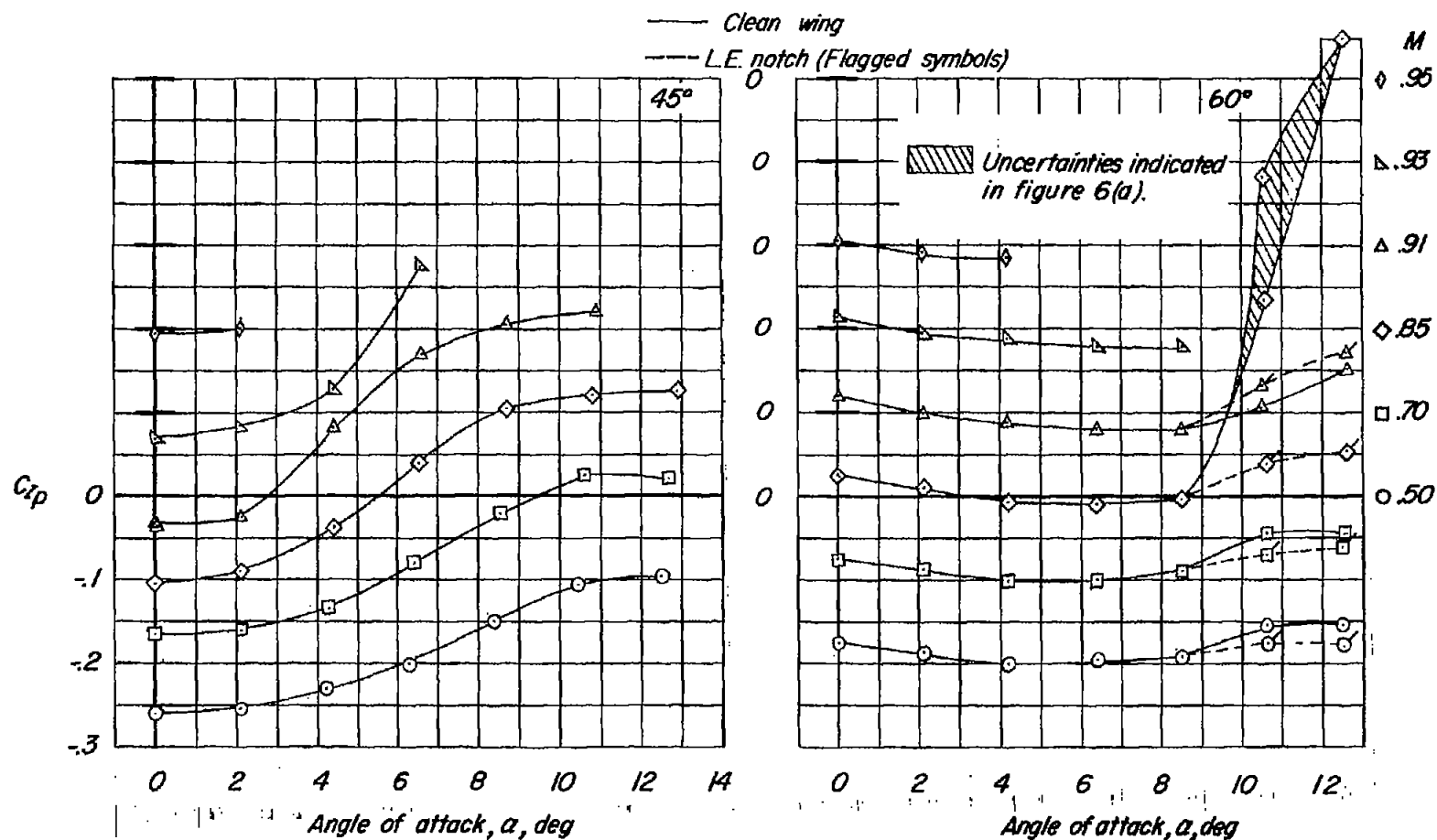
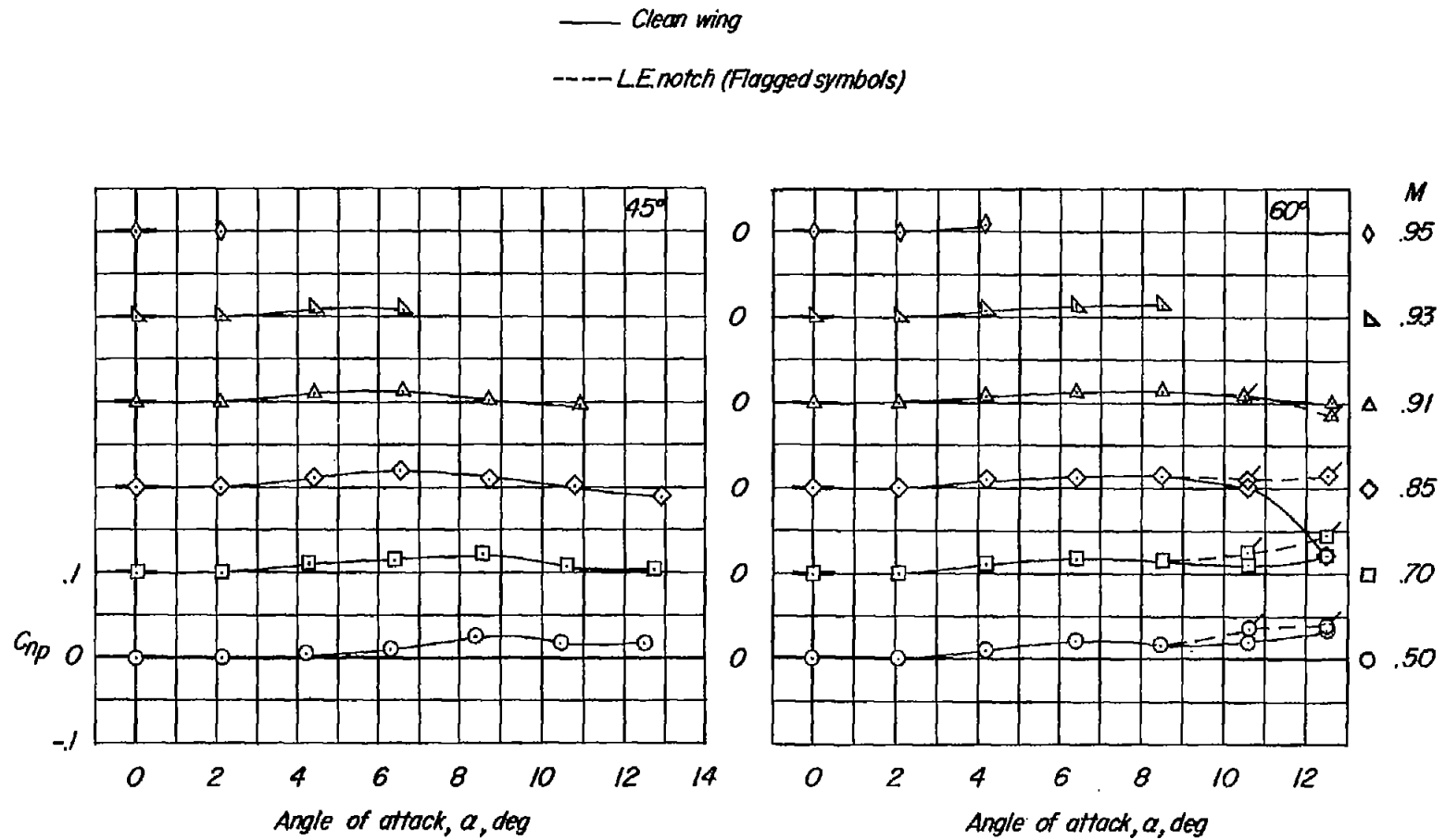
(a)  $C_{l_p}$ .

Figure 7.- Variation of the rolling derivatives  $C_{l_p}$ ,  $C_{n_p}$ , and  $C_{y_p}$  with angle of attack.  $\frac{pb}{2V} \approx 0$ .



(b)  $C_{np}$ .

Figure 7.- Continued.

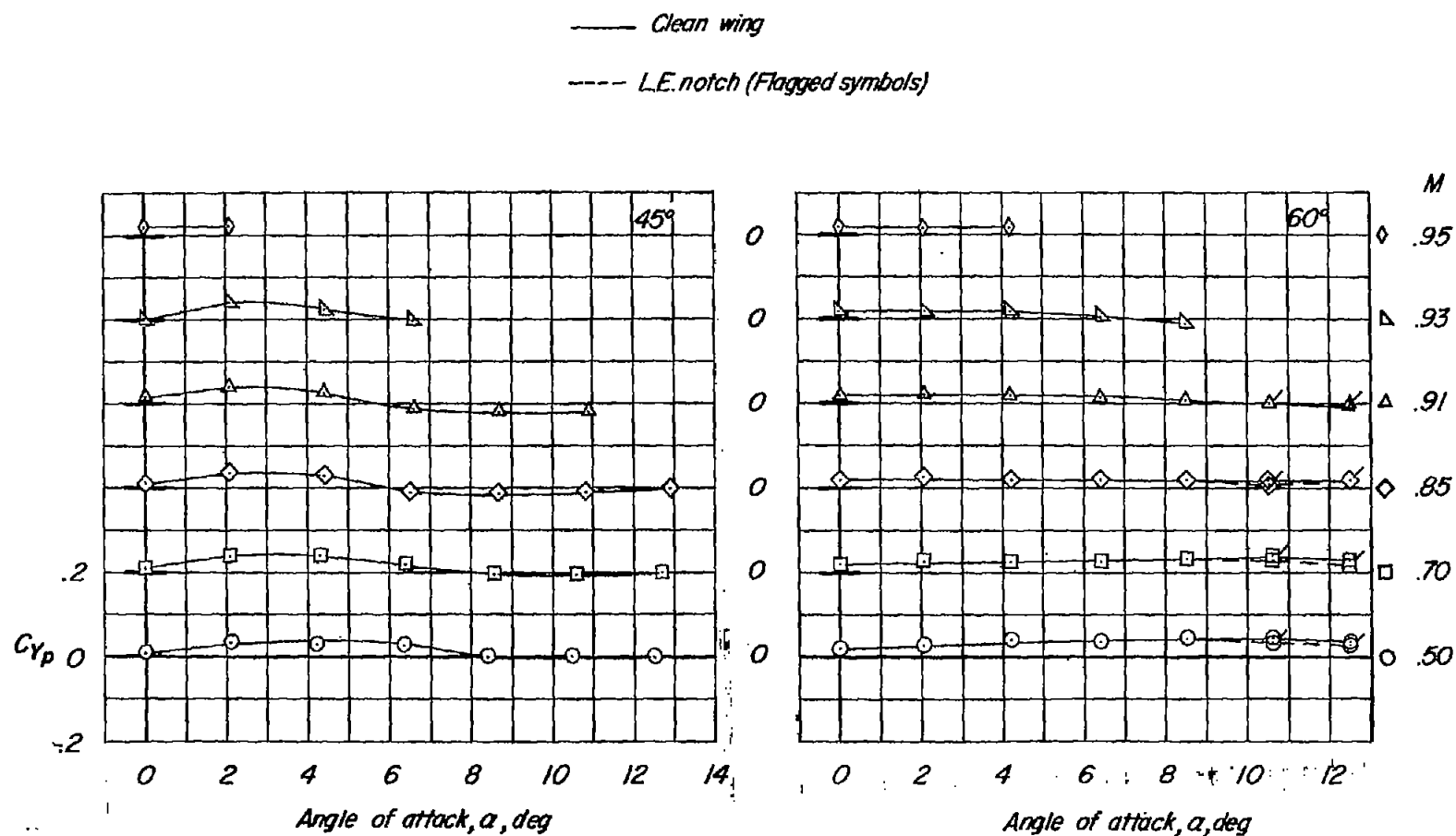
(c)  $C_{Yp}$ .

Figure 7.- Concluded.

$$\diamond \frac{pb}{2V} \approx 0$$

$$\circ \frac{pb}{2V} = \pm 0.6$$

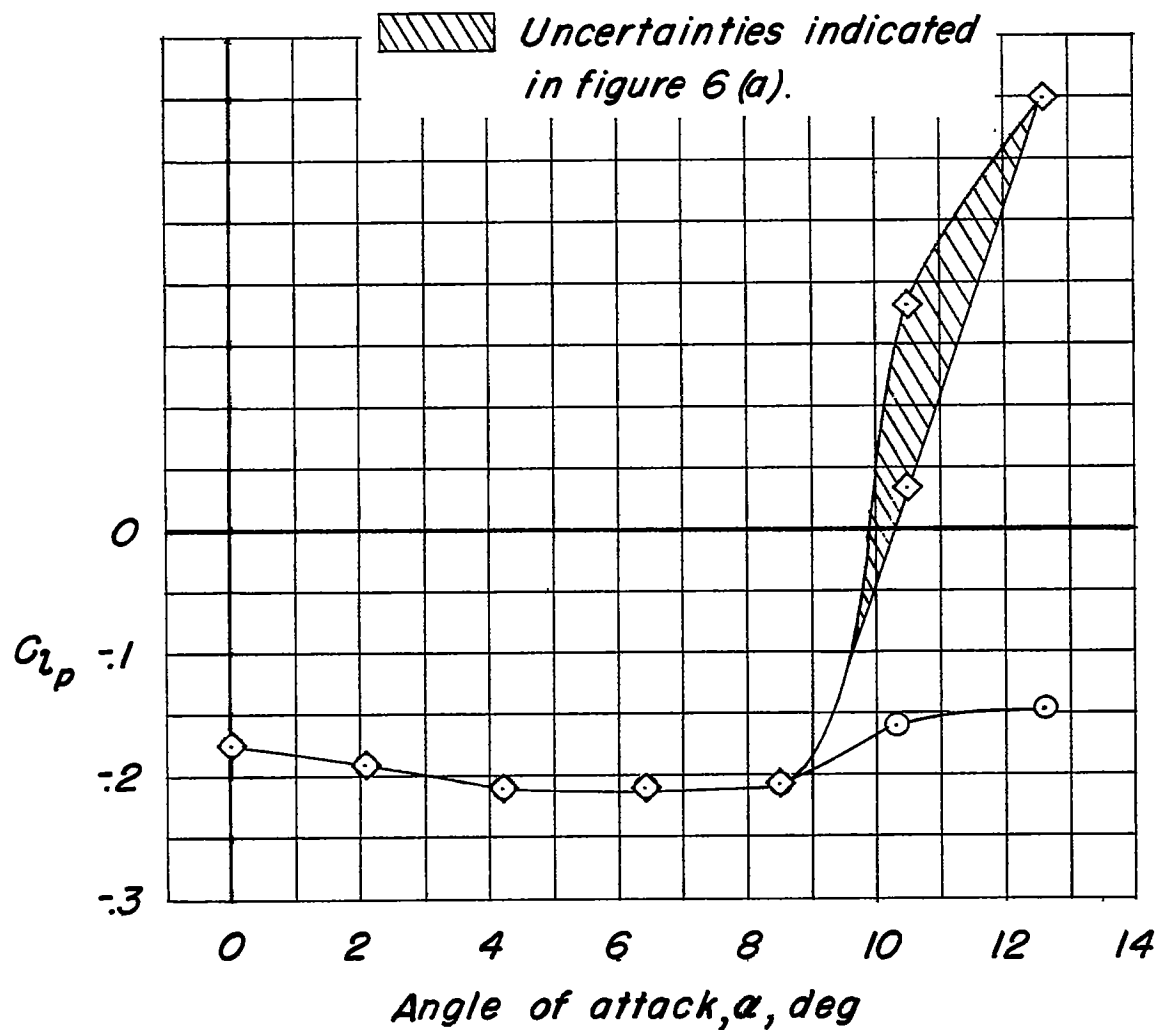


Figure 8.- Variation of  $C_{l_p}$  with angle of attack for the  $60^\circ$  (3-percent-thick) clean-wing configuration.  $M = 0.85$ .

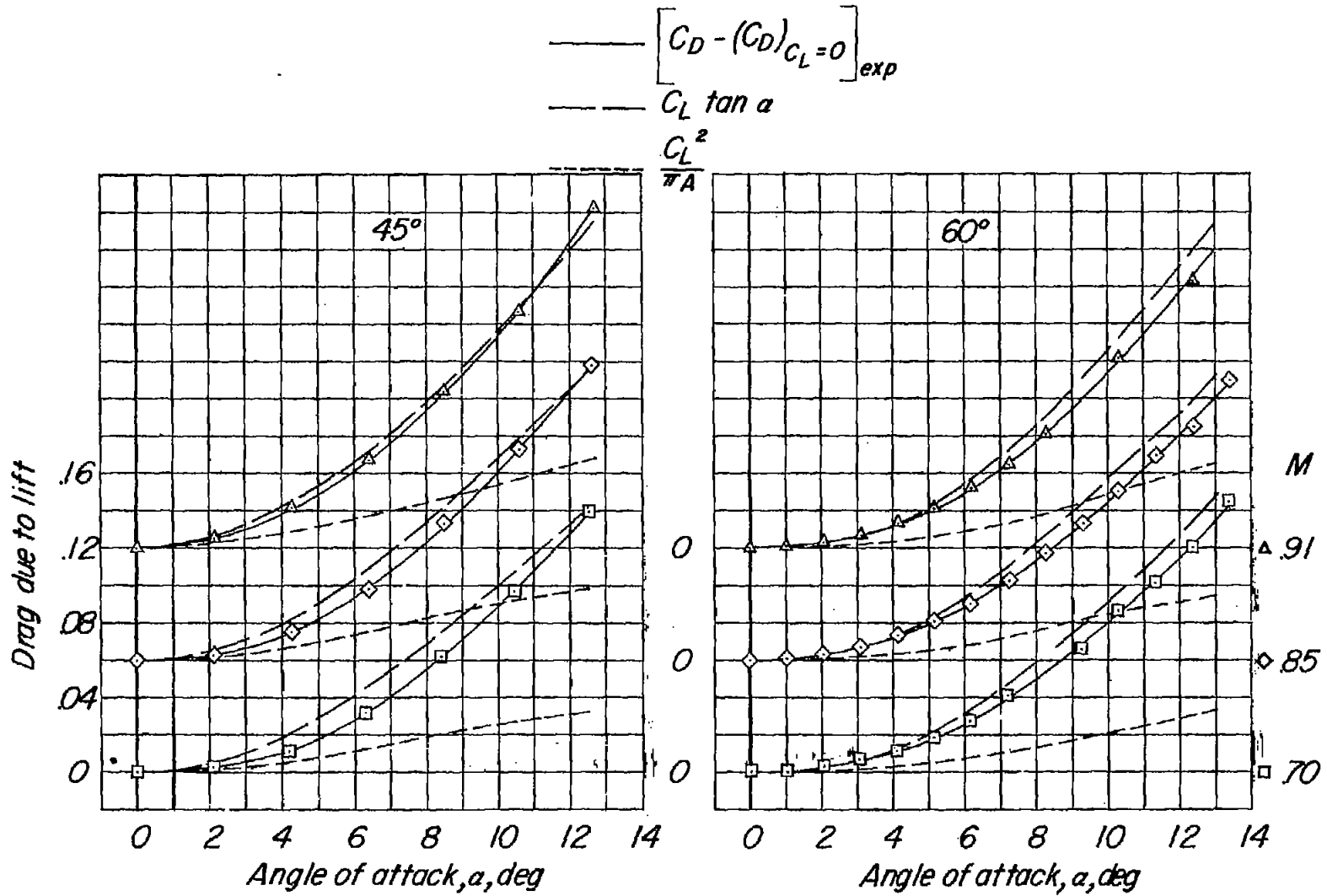


Figure 9.- Comparison of experimental and theoretical drag parameter for the two triangular wings.

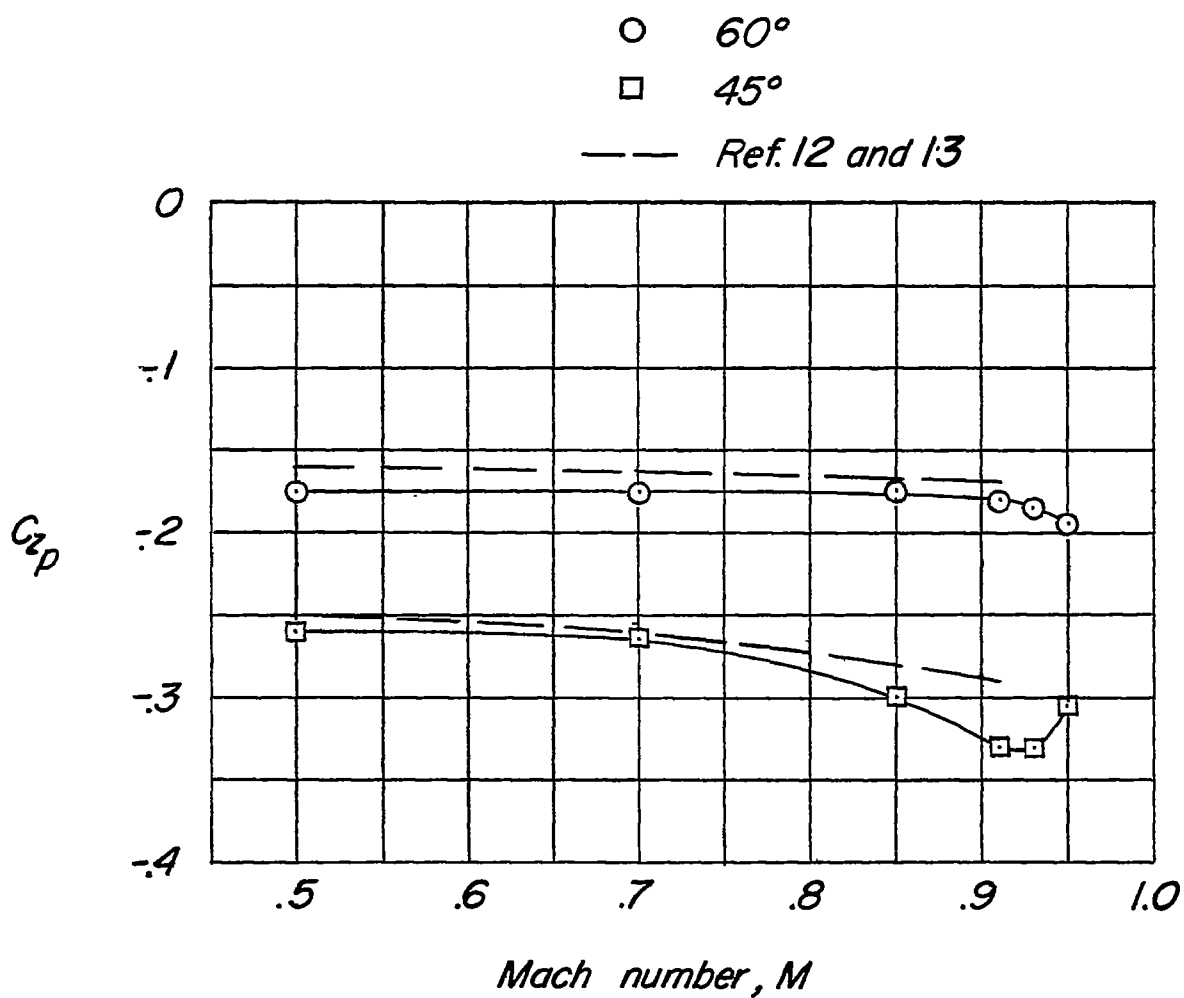


Figure 10.- Comparison of experimental and predicted variation of  $C_{zp}$  with Mach number for the two triangular wings.  $\alpha = 0^\circ$ .

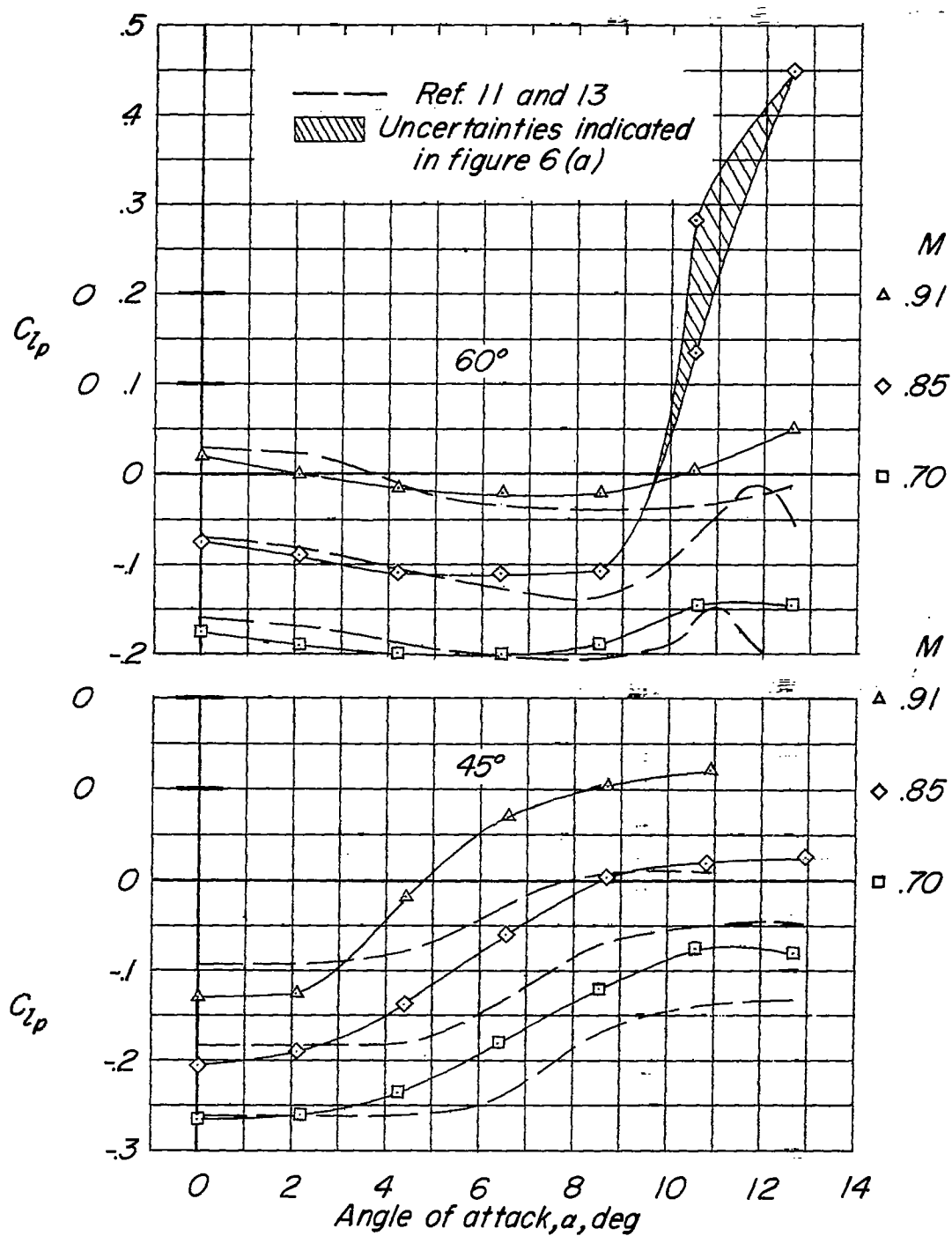


Figure 11.- Comparison of calculated and experimental variations of  $C_{lp}$  with angle of attack for the two triangular wings.  $\frac{pb}{2V} \approx 0$ .

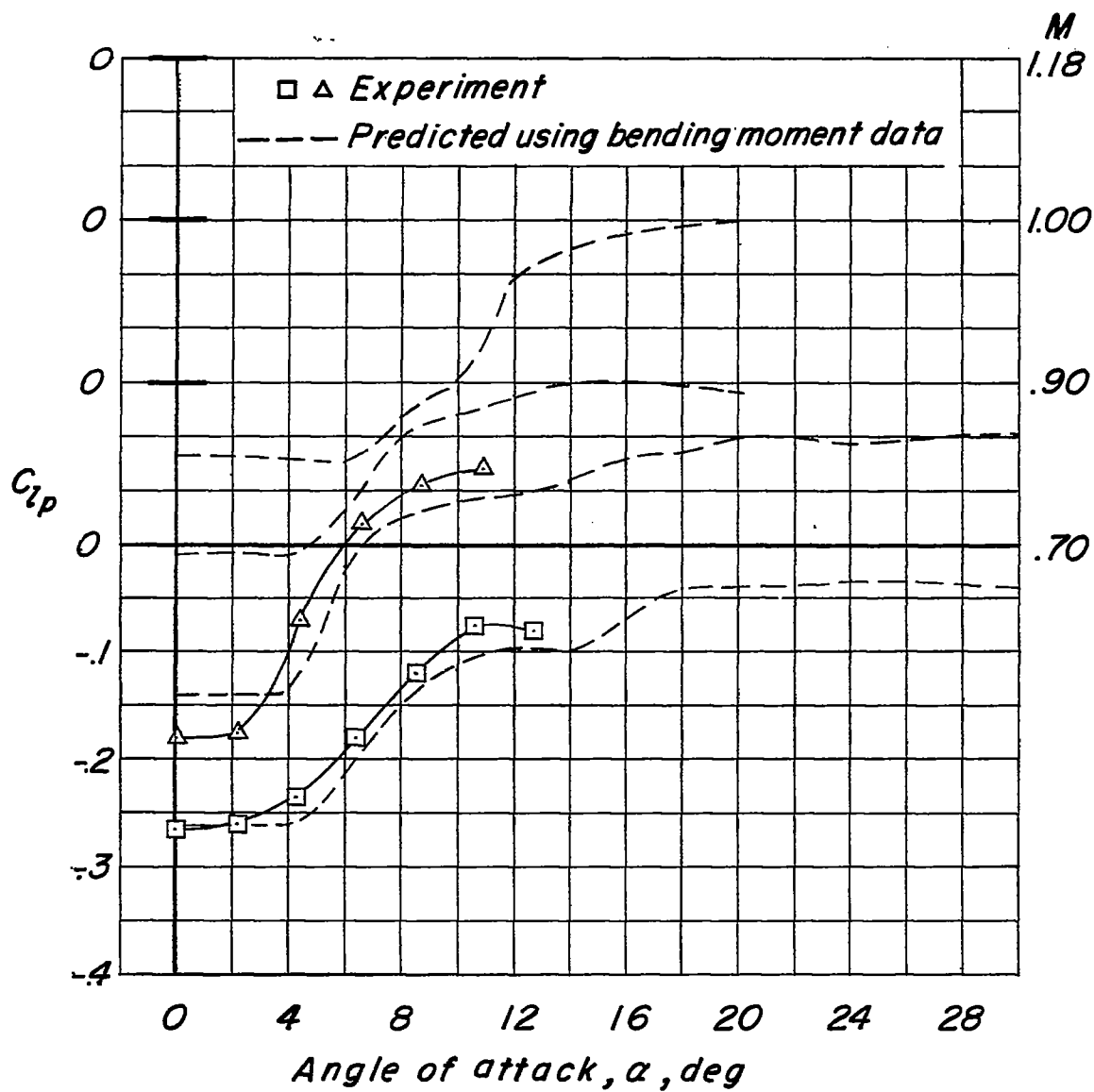


Figure 12.- Comparison of experimental and predicted values of  $C_{Lp}$  for the  $45^\circ$  triangular wing and extension of predicted values to large ranges of angle of attack and Mach number.

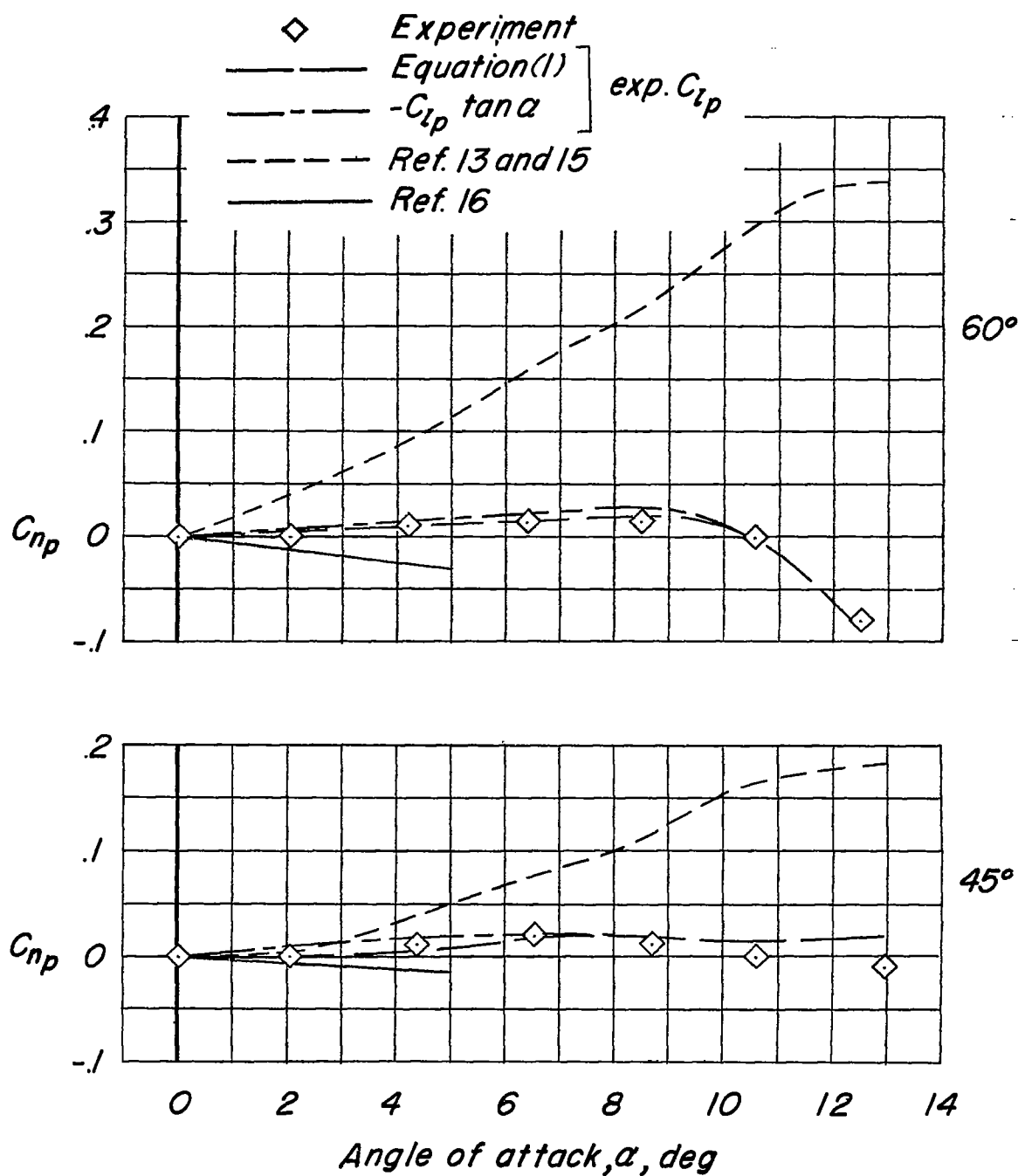


Figure 13.- Comparison of calculated and experimental variations of  $C_{np}$  with angle of attack for the two triangular wings.  $M = 0.85$ ;  $\frac{pb}{2V} \approx 0$ .

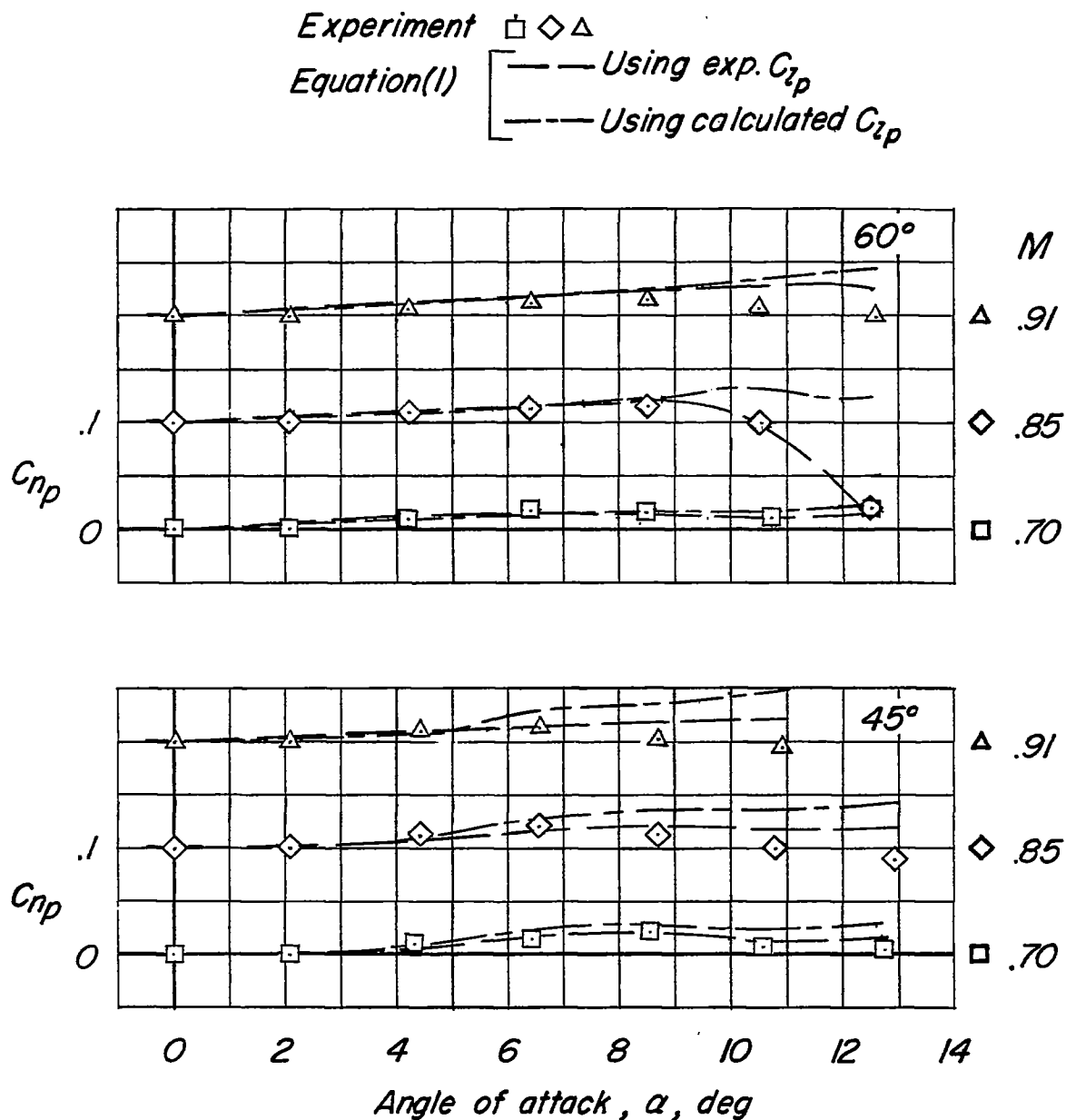


Figure 14.-- Comparisons of calculated and experimental variations of  $C_{np}$  with angle of attack for the two triangular wings.  $M = 0.85$ ;  $\frac{pb}{2V} \approx 0$ .

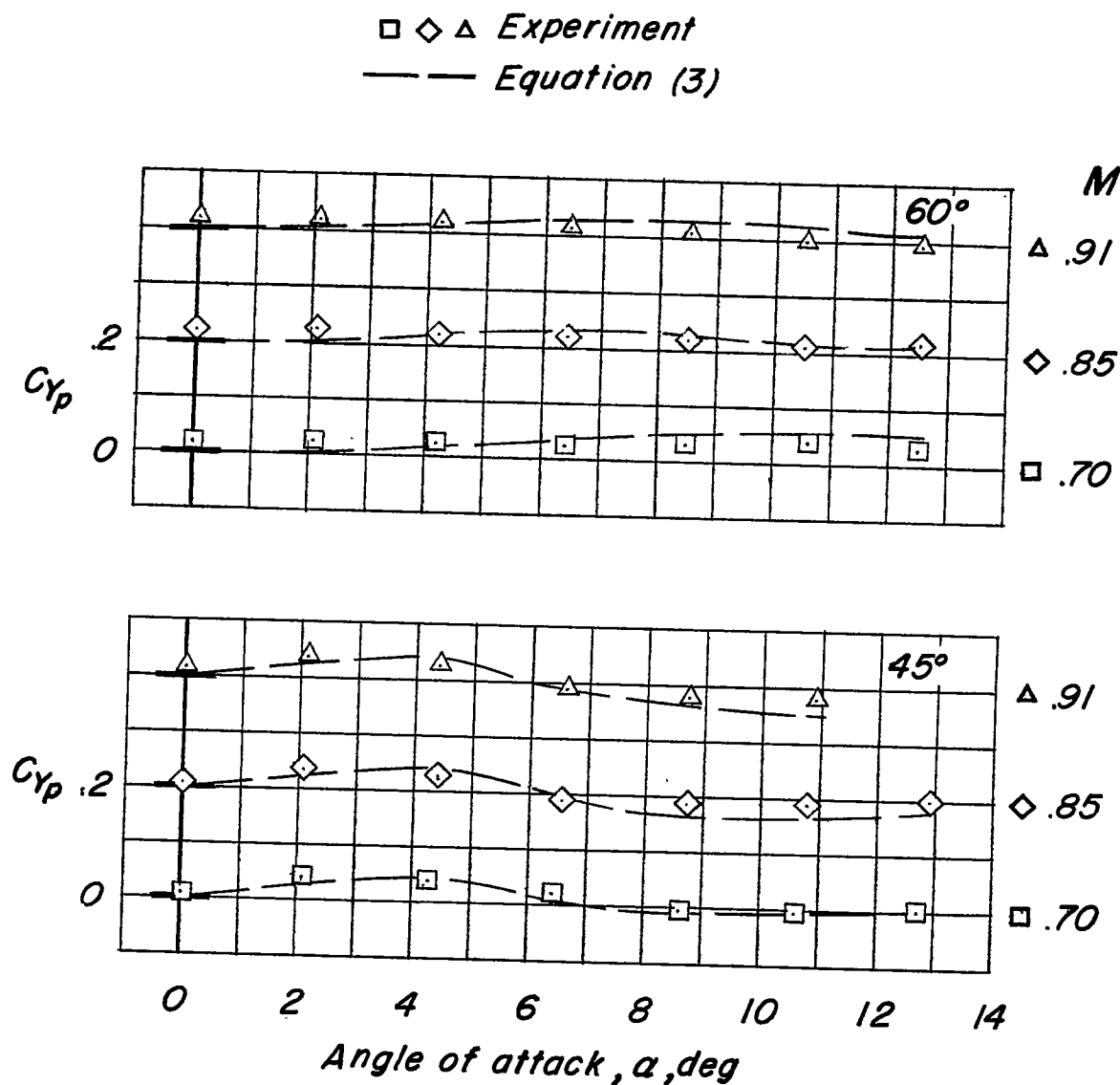


Figure 15.- Comparison of calculated and experimental variations of  $C_{yp}$  with angle of attack for the two triangular wings.